Degradation Mechanism and Relative Stability of Methylammonium Halide Based Perovskites Analyzed on the Basis of Acid Base Theory

doi: info:doi/10.1021/acsami.9b02374

ACS APPLIED MATERIALS & INTERFACES

Research Article

Cite This: ACS Appl. Mater. Interfaces 2019, 11, 12586−12593

www.acsami.org

Degradation Mechanism and Relative Stability of Methylammonium Halide Based Perovskites Analyzed on the Basis of Acid−Base Theory

Emilio J. Juarez-Perez,*[,†] Luis K. Ono,[†] Iciar Uriarte,[‡,§] Emilio J. Cocinero,[‡,§] and Yabing Qi*[,†]

[†]Energy Materials and Surface Sciences Unit (EMSSU), Okinawa Institute of Science and Technology Graduate University (OIST), 1919-1 Tancha, Onna-son, Okinawa 904-0495, Japan

[‡]Departamento de Química Física, Facultad de Ciencia y Tecnología, Universidad del País Vasco (UPV/EHU), Barrio Sarriena, 48940 Leioa, Spain

[§]Biofisika Institute (CSIC, UPV/EHU), Universidad del País Vasco (UPV/EHU), Apartado 644, E-48080 Bilbao, Spain

Supporting Information

ABSTRACT: The correct identification of all gases released during hybrid perovskite degradation is of great significance to develop strategies to extend the lifespan of any device based on this semiconductor. CH_3X (X = Br/I) is a released degradation gas/low boiling point liquid arising from methylammonium (MA^+) based perovskites, which has been largely overlooked in the literature focusing on stability of perovskite solar cells. Herein, we present an unambiguous identification of CH_3I release using microwave (rotational) spectroscopy. An experimental back-reaction test demonstrates that the well-known CH_3NH_2/HX degradation route may not be the ultimate degradation pathway of $MAPbX_3$ in thermodynamic closed systems. Meanwhile, the CH_3X/NH_3 route cannot back-react selectively to MAX formation as occurred for the former back-reaction. Metadynamics calculations uncover the X halide effect on energy barriers for both degradation reactions showing a better stability of Br based perovskite ascribed to two aspects: (i) lower Brönsted−Lowry acidity of HBr compared to HI and (ii) higher nucleophilic character of CH_3NH_2 compared to NH_3. The latter property makes CH_3NH_2 molecules stay preferentially attached on the electrophilic perovskite surface (Pb^{2+}) during the dynamic simulation instead of being detached as observed for the NH_3 molecule.

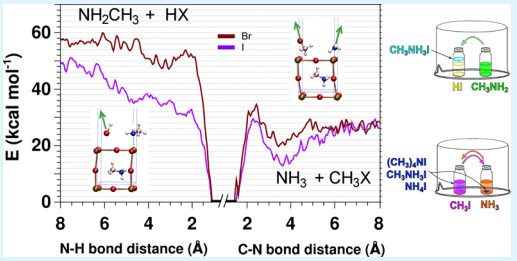

KEYWORDS: *methylammonium lead iodide, degradation, methyliodide, methylamine, rotational spectroscopy, metadynamics calculations, perovskite solar cells*

INTRODUCTION

Currently, long term operational stability can be considered one of the major issues for the future of perovskite solar cell technology.[1] Even several research groups around the world have already surpassed the 20% power conversion efficiency in their devices, and initial signs of success on the long term stability of perovskite solar cells are appealing lately.[2] The truth is that the operational device stability tests longer than 1000 h at a maximum power point are still scarcely reported.[3] The methylammonium ion (MA^+) is ubiquitous in hybrid perovskite chemical formulations as one of the organic cations more used in the A site of the perovskite structure.[4] MA^+ was in the inception of the field,[5] and it has been used in every efficiency record reported[6] as a solitary cation or mixed with other organic (FA^+) or inorganic (Cs^+) monovalent cations.[4] However, there is an enigma on elucidating how MA^+ based hybrid perovskite degrades and what are the gas products of degradation when the perovskite decomposes. Meanwhile, it is widely accepted that there is PbI_2 solid state phase remaining after degradation of $CH_3NH_3PbI_3$ ($MAPbI_3$).[7] There is no experimental evidence of CH_3NH_3I (MAI) salt formation as a separated phase after perovskite degradation. The absence of such a solid state product of degradation provides clues that decomposition by-products of MA^+ were released in gas phase. The correct identification of these released gases is of great significance to prevent degradation and extend the durability of the MA^+ based perovskite solar cells. For instance, it could determine the best strategy for device encapsulation.[8,9] Ultimately, these studies would reveal whether a MA^+ based perovskite will meet the required lifetime operational stability for commercial solar cells.

Early in the hybrid halide perovskite literature, it was proposed that $MAPbI_3$ formally loses a methylammonium cation $[CH_3NH_3]^+$ (MA^+) and iodide anion $[I]^-$ during decomposition and they are released as neutral methylamine (CH_3NH_2) and hydrogen iodide (HI) gases.[10−13] Frequently, water and oxygen are considered as agents favoring the irreversible perovskite decomposition, although monohydration of hybrid perovskite has been demonstrated as a fully reversible

Received: February 5, 2019
Accepted: March 8, 2019
Published: March 8, 2019

DOI: 10.1021/acsami.9b02374
ACS Appl. Mater. Interfaces 2019, 11, 12586−12593

process.[14] However, it was found that encapsulation and inert conditions do not avoid perovskite decomposition.[7,15,16] In contrast with this early assumption of CH_3NH_2 + HI release, it was later discovered experimentally that, during the high temperature thermal degradation route of $MAPbI_3$, the main gases released before PbI_2 thermal evaporation are CH_3I and NH_3.[17−20] Early in 2014, Williams et al. found that MAI could decompose via the CH_3I/NH_3 route according to in situ FTIR gas measurements.[18] Later, McLeod et al. found intermediate compounds based on CH_3I and NH_3 as suggested by NMR and XPS studies.[19,21] Finally, Juarez-Perez et al. carried out more unambiguous coupled mass spectrometry/thermogravimetry analysis demonstrating that the high temperature thermal degradation of MAI and $MAPbI_3$ at inert and anaerobic atmospheric pressure conditions (He gas flow) produces neatly CH_3I/NH_3 as gas products of degradation while the CH_3NH_2/HI pair is not observed.[17] More recently, it has been found that both degradation routes (CH_3NH_2 + HX and CH_3X + NH_3) take place simultaneously near ambient temperature and vacuum conditions.[20,22] Under such different temperature condition experiments, the release of CH_3I + NH_3 is understood as the thermodynamically favored path of degradation and the CH_3NH_2 + HI release is a kinetically favored process. Similarly but not exactly identical in terms of temperature thresholds, $MAPbBr_3$ has also demonstrated to degrade by both pathways.[22]

In this work, we report (1) the unambiguous detection of released gases during thermal degradation of $MAPbI_3$ by high-resolution rotational spectroscopy, (2) proof-of-concept back-reaction experiments for the degradation process in perovskites using the known gas products of degradation as reagents, and (3) a set of first principles metadynamics calculations to study the energy coordinate paths of formation and degradation of the MA^+ cation depending on the halide X anion involved (Br^- or I^-) on the hybrid $MAPbX_3$ perovskite surface.

RESULTS AND DISCUSSION

How Is It Possible that There Are Two Different Routes of Degradation in MA^+ Halide Compounds? The Chemical Reaction Paths Connecting Monovalent Quaternary Ammonium, Neutral Methylamine, and Neutral Methyliodide Molecular Entities. One of the goals of this work is to understand how MA^+ based halide organic salts (including perovskites) can undergo two different experimentally observed degradation paths depending on the temperature and pressure conditions. Ammonium (A^+, Figure 1a) and tetramethylammonium (QA^+, Figure 1c) cations are exemplary models of quaternary amine cations showing two extreme situations with nonsubstituted and fully methyl substituted quaternary N atoms, respectively. Both are examples of quaternary amines having only one degradation route because the N center is bonded to only one kind of substitution, H (hydrogen atom) or CH_3 (methyl group), respectively. In comparison, the quaternary nitrogen in MA^+ is simultaneously substituted by one methyl and three hydrogen atoms (see Figure 1b).

The route described in Figure 1a for AI is the reverse of the acid−base neutralization to form the AI salt itself. In contrast, reaction in Figure 1c is the reverse Menshutkin reaction (the reverse of tertiary amine alkylation reaction) between CH_3I and Lewis base $(CH_3)_3N$ (trimethylamine). Because the N atom in MA^+ is substituted by three protons and a methyl moiety, MA^+ has the ability to undergo both paths of reaction depicted as b.1 and b.2 in Figure 1. Note that, for the MA^+ cation case, reaction

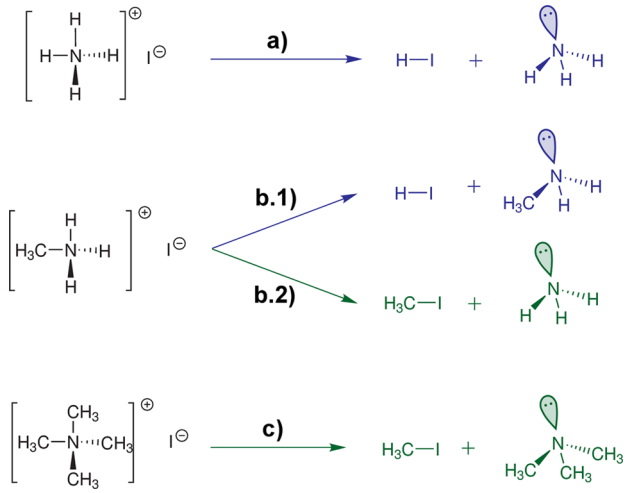

Figure 1. Degradation reaction routes for (a) ammonium iodide (AI), (b) methylammonium iodide (MAI), and (c) tetramethylammonium iodide (QAI). Reaction in panel (b) splits depending if the product of degradation is (b.1) CH_3NH_2 + HI or (b.2) CH_3I + NH_3. The blue color depicts a reaction, which is the reverse of acid−base neutralization. The green color depicts the reverse Menshutkin reaction type.

b.1 is three times more likely to occur than reaction b.2 if guessing an identical energy pathway for both reactions. In the following sections, proof of the existence of both decomposition routes (b.1 and b2) is provided by using rotational spectroscopy; a set of experimental back-reaction tests using CH_3NH_2 + HI and CH_3I + NH_3 as gas reagents are carried out to analyze all solid products back-generated; finally, metadynamics calculations uncovered the coordinate of reaction and energy pathway describing b.1 and b.2 type degradation routes for $MAPbX_3$ based perovskite (X: Br or I).

Rotational Spectroscopy Analysis Results. Rotational or microwave spectroscopy studies the resonant transitions between molecular rotational levels, and it provides the most accurate view of the molecular structure although it is restricted to molecules with permanent dipole moments.[23] The great advantage of this technique is its extremely high resolution that allows unambiguous discrimination even between different isomers, whether tautomers, conformers, isotopomers, or enantiomers. The error in the position of spectral lines is typically a few kilohertz, which in wavenumber units corresponds to 0.000001 cm^{-1}. This is several orders of magnitude smaller than the typical spectral resolution achieved with techniques based on infrared spectroscopy. Rotational spectroscopy has been traditionally used to explore the conformational landscape of small- to medium-sized molecular systems in the gas phase.[24,25] The unambiguous identification of products is the key feature that makes rotational spectroscopy a powerful tool in cases where other analytical techniques may struggle. In this work, we use rotational spectroscopy to provide an unambiguous identification of the CH_3I and CH_3NH_2 gas products released upon heating progressively a MA based perovskite sample.

The results of this experiment can be found in Figure 2. It can be observed that the first traces of both CH_3I and CH_3NH_2 appear when the sample is heated at 200 °C. Further prolonging to 70 h at 230 °C improves the signal-to-noise ratio of these rotational transitions. A total of nine and three transitions were unequivocally identified in the spectrum for CH_3NH_2 and CH_3I,

DOI: 10.1021/acsami.9b02374
ACS Appl. Mater. Interfaces 2019, 11, 12586−12593

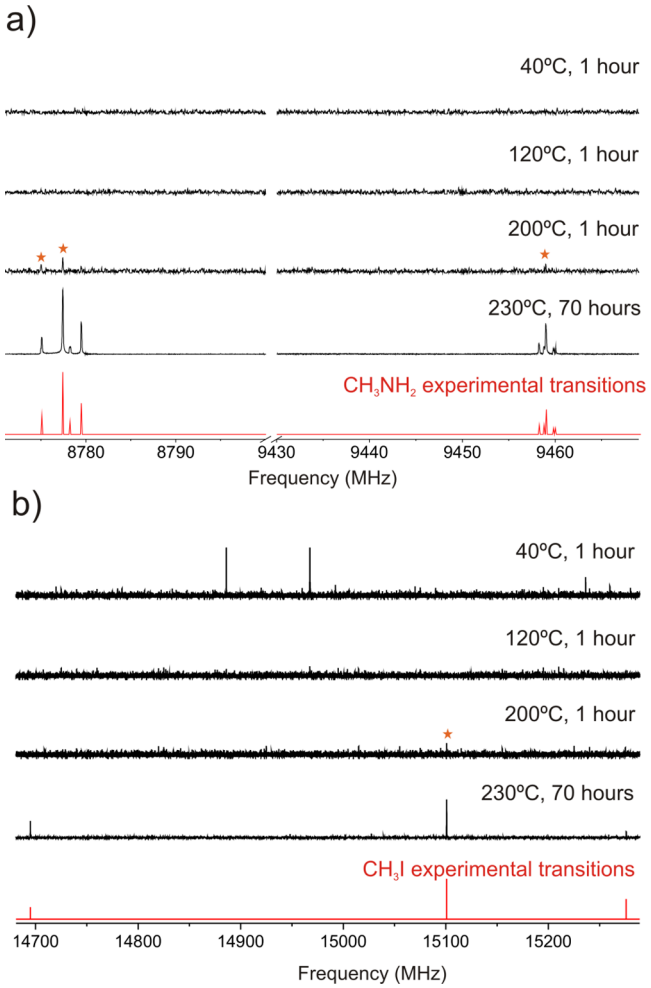

Figure 2. In black, sections of the experimental rotational spectrum obtained after heating $MAPbI_3$ as a function of temperature and time. Red stars mark the first appearance of lines corresponding to CH_3I or CH_3NH_2. In red, positions of the rotational transitions of CH_3I and CH_3NH_2 reported in the literature. The two peaks at 40 °C probably correspond to an unidentified volatile impurity related to the adsorbed solvent that evaporates at lower temperatures.[18,22,26] (a) Frequency region corresponding to the transitions of CH_3NH_2 as reported in the literature.[27] (b) Frequency region corresponding to the transitions of CH_3I as reported in the literature.[28]

respectively. These results unambiguously confirm that both CH_3NH_2 and CH_3I are released upon heating $MAPbI_3$ under inert conditions as represented by degradation pathways b.1 and b.2 in Figure 1. In addition, although the spectrum should be normalized by the dipolar moments, it can be qualitatively observed that there would be a greater release of CH_3NH_2 than CH_3I. However, quantification of the reaction extension and thermal analysis is not easy to accomplish using rotational spectroscopy. Instead, two independent works reported such quantification using mass spectrometry (MS) elsewhere.[20,22] For instance, the CH_3I/CH_3NH_2 molecular ratio describing the extension for each decomposition reaction reaches ~0.12 maximum during a light/heat pulse of 55 mW cm^{-2} (T ~70 °C).[22] For completeness, m/z ratios for CH_3I, NH_3, NH_2CH_3, and HI species depending of the $MAPbI_3$ sample heating temperature are included in Figure S1 noting the earlier release of such species at 50−60 °C.

MAI Formation Using the Gas Degradation Products as Precursors. It was recognized that a MA^+ cation can undergo both chemical transformation paths because there are two types of substituents in its N atom (Figure 1) and it has been irrefutably demonstrated using rotational spectroscopy (Figure 2). Now, it is interesting to prove if such gases (CH_3NH_2 + HI or CH_3I + NH_3) are able to synthesize back MAI to study further the reversibility/irreversibility properties of such degradation reactions.

MAI organic salts for hybrid perovskite synthesis are usually prepared in high yield mixing commercial methylamine solution (33 wt %) in ethanol and hydroiodic acid (57 wt %) in water without dilution.[29] CH_3NH_2 and HI reagents are gases at room temperature and pressure, but commercially they are better available as dissolved gases in a solvent typically ethanol or water. The strong acid−middle strong base neutralization reaction producing MAI is

$$HI + CH_3NH_2 \rightarrow CH_3NH_3I \quad (1)$$

Here, an experimental setup to carry out this neutralization reaction exclusively in gas phase is prepared consisting of two small bottles containing the commercial solutions and separated next to each other inside a sealed beaker (see Figure 3a and Figure S2a). After a few minutes, a solid white ring is observed on the top of the HI solution containing glass bottle. This white solid is a high purity MAI formed by gas phase reaction of CH_3NH_2 and HI molecules evaporated from the corresponding solutions. Figure S2a shows a time-frame photographic sequence, and Figure S3 shows a Rietveld refinement analysis of the obtained white solid product. This simple even naive

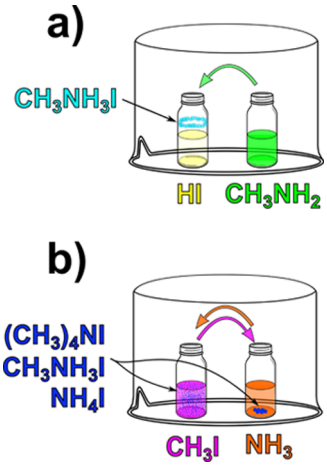

Figure 3. Cartoon illustrating the reagents and products obtained in the gas phase reactions. (a) Experiment demonstrating MAI formation using vapors of HI and CH_3NH_2 solutions. A white solid ring appears on the top surface of the solution. (b) Experiment using CH_3I solvent grade (left) and ammonia solution (NH_4OH, right). A white fine solid precipitates forming a suspension in the CH_3I bottle. Larger precipitation appears in the bottom of the ammonia solution bottle. The three crystalline solids obtained in the experiments are further analyzed and phase quantified by Rietveld refinement (see the Supporting Information for further details). Briefly here using bold numbers, the results are for experiment in panel (a); all of the solid material is 100 wt % MAI. The solid precipitate in the experiment in panel (b) in the CH_3I containing bottle is 50 wt % QAI, 20 wt % MAI, and 30 wt % AI. The solid precipitate in the experiment in panel (b) in the NH_3 containing bottle is 70 wt % QAI, 20 wt % MAI, and 10 wt % AI.

DOI: 10.1021/acsami.9b02374
ACS Appl. Mater. Interfaces 2019, 11, 12586−12593

experiment illustrates clearly the high reversibility of CH_3NH_2 and HI reacting back to MAI synthesis. Therefore, the release of CH_3NH_2 and HI molecules from a MA based perovskite should be not considered as a degradation reaction if such perovskite is inside a thermodynamic closed system (where CH_3NH_2 and HI definitely cannot escape). Furthermore, this reversibility implies that, in the presence of PbI_2, the back-reaction inevitably leads to the synthesis of $MAPbI_3$ (e.g., the VASP method[30]). In fact, CH_3NH_2 and HI gases have been already demonstrated as excellent reagents used directly in gas phase to synthesize $MAPbI_3$ perovskite.[31−33] Therefore, not only a thermodynamic closed system for perovskite is the mandatory first premise to guarantee device stability, but also it is needed that the released gases at working temperatures are not undergoing irreversible degradation or no-selective back-reaction to MAX. Only then, the reversible process can be used to sustain a prolonged stability of the device in time.

Similar to the above test, another experiment was performed but using instead NH_3 aqueous solution and CH_3I reagent grade solvent in two small bottles arranged separated next to each other inside a sealed beaker (see Figure 3b). After a few minutes, fine white solid powders precipitate inside the CH_3I containing bottle. Later, bigger crystals are observed in the NH_3 solution containing bottle (see Figure S2b). Contrary to the CH_3NH_2/HI experiment, powder XRD phase quantification in this experiment determines that the white solid is actually a mixture of QAI, MAI, and AI salts (reaction 2) (see Rietveld refinement analysis in Figures S4 and S5).

$$CH_3I + NH_3 \rightarrow N(CH_3)_4I + CH_3NH_3I + NH_4I \quad (2)$$

The relative quantity of each salt formed depends on whether NH_3 molecules react in an environment with a rich excess of CH_3I molecules (left bottle) or CH_3I molecules react with an excess of NH_3 molecules (right bottle). In any case, the most relevant fact demonstrated in this experiment is that these reagents $CH_3I + NH_3$ do not lead exclusively to MAI as in the first experiment using CH_3NH_2 + HI. Instead, CH_3I and NH_3 react forming a significant quantity of QAI and AI. It is mainly because the NH_3 molecule is methylated by CH_3I as many times as possible and not only once to produce exclusively MAI. We assume that the plausible release of CH_3I/NH_3 from perovskite is a 1:1 ratio but this stoichiometric ratio could not impede the ammonia permethylation because a majority of QAI formation is observed independent of the two extreme limiting reagent situations around each bottle. A simplified mechanism can be represented by chemical reaction 3

$$MAI + 3(CH_3I + NH_3) \rightarrow QAI + 3AI \quad (3)$$

The presence of the permethylated ammonium cation during thermal degradation of $MAPbI_3$ and MAI was already demonstrated experimentally but not quantified.[17]

In essence, these two basic experiments represent the stability problem of all MA^+ based hybrid perovskites. Generalizing for X = I or Br, CH_3X and NH_3 are the authentic early degradation products of MA^+ based hybrid perovskites. CH_3X and NH_3 cannot synthesize back easily and exclusively (selectively) to MAX. Therefore, CH_3X and NH_3 could (1) be released out in thermodynamically open systems or (2) react further forming QA^+ and A^+ based perovskites in a closed system (not useful material with light harvesting properties), or (3) CH_3X could polymerize to polyethylene-like compounds as observed in the work by Ke et al.[34] assuming an iodine-transfer polymerization reaction for CH_3I.[22] In addition, the fact that the CH_3X and NH_3 transformation is less significant in quantity than production of CH_3NH_2 and HX does not matter. The law of mass action and Le Chatelier's principle anticipate that the system will readjust to counteract the chemical imbalance continuously shifted by the disappearance of CH_3X and NH_3 until total MA^+ based perovskite exhaustion.

Metadynamics Calculations on Periodic Hybrid $MAPbX_3$ Perovskite Surface. In the following, we will discuss a theoretical approach to compare the energy paths of reaction in $MAPbX_3$ surfaces releasing CH_3NH_2/HX or CH_3X/NH_3 to uncover the X halide effect on energy barriers for both reactions.

Metadynamics is a tool for exploring free energy landscapes of chemical reactions. Metadynamics is based on molecular dynamics (MD) methods, and it can be applied in combination with first principles dynamics methods, in particular with the DFT based Car−Parrinello molecular dynamics.[35−37] The profile of the free energy landscape for a reaction gives us information about the energetics of the transformation between reactants and products and therefore about the direction of the process. By using conventional MD methods, the probability to observe the system carrying out a chemical transformation during the simulation is extremely low, and it needs a long time of expensive simulation. Such a probability decreases exponentially in relation with the energy barrier height to surpass during such chemical transformation between stable states. Metadynamics methods solve this problem of rare event observation by increasing this probability adding small potential energy instability packets (gaussians) into the chemical bond, angle, coordination number, or whatever geometrical collective variable under study in the ground state configuration. By adding this small potential energy instability, the system artificially avoids revisiting again the most stable configuration of the system pushing up to search for another more stable configuration. At some point after adding enough potential energy instability, the system suffers from the definitive modification accounted by the collective variable. Then, a free energy landscape of the reaction is obtained as the reverse of the destabilizing growing history of potential energy added.

Metadynamics calculations using a simple model represented by one isolated ionic par system $MA^+\cdots X^-$ can be useful to describe the main trends of the chemical behavior of the organic part of $MAPbX_3$ perovskite (see the Theoretical Calculations on Simplified Model section in the Supporting Information). However, the chemical environment observed by one MA^+ on the $MAPbX_3$ surface is significantly different from the vacuum surroundings observed by one isolated ionic par system $MA^+\cdots X^-$. It could affect in an unpredicted way the free energy versus reaction coordinate in the reactions suffered by MA^+. Therefore, the metadynamics calculations were carried out on the model surface of hybrid perovskite. The periodic simulated system of choice in this case consists of the cubic phase of $MAPbX_3$ with one of the (0 0 1) planes interfaced with 20 Å vacuum space available for released gaseous species. Cubic phase perovskites are chosen for both cases (X = Br and I) for simplicity in calculations. Therefore, metadynamics calculations are set to a constant temperature of 340 K ($MAPbI_3$ is a tetragonal phase below 330 K). On the top of this surface there is a $CH_3NH_3^+$ ion, and metadynamics calculations are carried out in this entity choosing the corresponding collective variable. The reaction able to produce CH_3NH_2 + HX is formally described as

$$CH_3NH_3PbX_3 \rightarrow CH_3NH_2 + HX + PbI_2 \quad (4)$$

DOI: 10.1021/acsami.9b02374
ACS Appl. Mater. Interfaces 2019, 11, 12586−12593

where one of the N−H bond distances in the top surface $CH_3NH_3^+$ cation is selected as the collective variable. The reaction releasing $CH_3X + NH_3$ is

$$CH_3NH_3PbX_3 \rightarrow CH_3X + NH_3 + PbI_2 \quad (5)$$

where the collective variable for this reaction is the C−N bond distance of the $CH_3NH_3^+$ cation. Free energy paths for both reactions are obtained by recording the corresponding collective variables for $MAPbX_3$ with X = Br and I as can be seen in Figure 4.

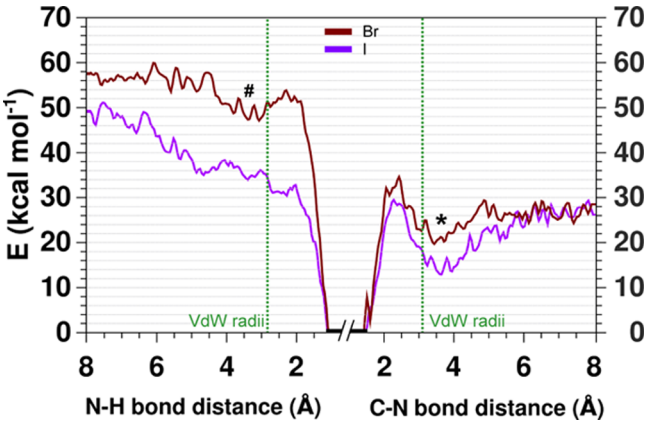

Figure 4. Free energy versus collective variable distance paths studied in the framework of metadynamics for reactions 4 (left side) and 5 (right side) with X = Br (crimson) and I (violet). Van der Waals radii (sum of the atoms involved in reaction) are depicted for each case as green dotted lines. Crimson and violet thick lines represent the energy paths for $MAPbX_3$ decomposition with X = Br and I, respectively. # and * symbols are placed in local minima stable energy valleys.

The energy profile path obtained by metadynamics calculations for reaction 4 producing CH_3NH_2 and HX indicates mostly reversible reaction, since the free energy path in Figure 4 is monotonically increasing in the studied interval of N−H bond distances. Noteworthy, the reaction producing CH_3NH_2 and HBr contains a shallow energy valley marked with the # symbol in Figure 4. Such shallow energy means that CH_3NH_2 + HBr could have a longer lifetime as species compared to the CH_3NH_2 + HI pair. The reason why the Br system can afford such a situation is ascribed to the higher basicity of the Br^- conjugated base compared with its I^- counterpart. On the other hand, the calculated energy profile path of reaction 5 releasing $CH_3X + NH_3$ favors irreversible reaction. The calculated path shows an activation energy barrier of 30 (35) kcal mol^{-1} for the I (Br) system following a reverse Menshutkin reaction direction or 18 (14) kcal mol^{-1} for direct Menshutkin reaction. Therefore, the $CH_3X + NH_3$ pair is a thermodynamic product of the decomposition reaction compared to CH_3NH_2 + HX, but the energy barriers and the existence of local minima (stable energy valleys) (denoted in Figure 4 as # and *) may play a role in the extension of each reaction at low temperature. After transformation to $CH_3X + NH_3$, the energy local minimum (marked as * in Figure 4) appears ~5 kcal mol^{-1} deeper in energy for the I system than the Br system. According to these calculated energy paths, it is better understood that experimentally under high temperature (>360 °C) all products of degradation are obtained via reaction 5 (the thermodynamic products) irrespective of X = Br[22] or I.[17] Meanwhile, rotational spectroscopy measurements in this work carried out at middle temperature degradation tests (<230 °C) showed both degradation routes for $MAPbI_3$. Finally, at low temperature close to the maximum temperature of operation for PV devices (~70 °C), $MAPbI_3$ still degrades via both paths,[20,22] but $MAPbBr_3$ only releases the kinetic products CH_3NH_2 and HBr.[22] According to these metadynamics results, $MAPbI_3$ is more unstable than $MAPbBr_3$ because of

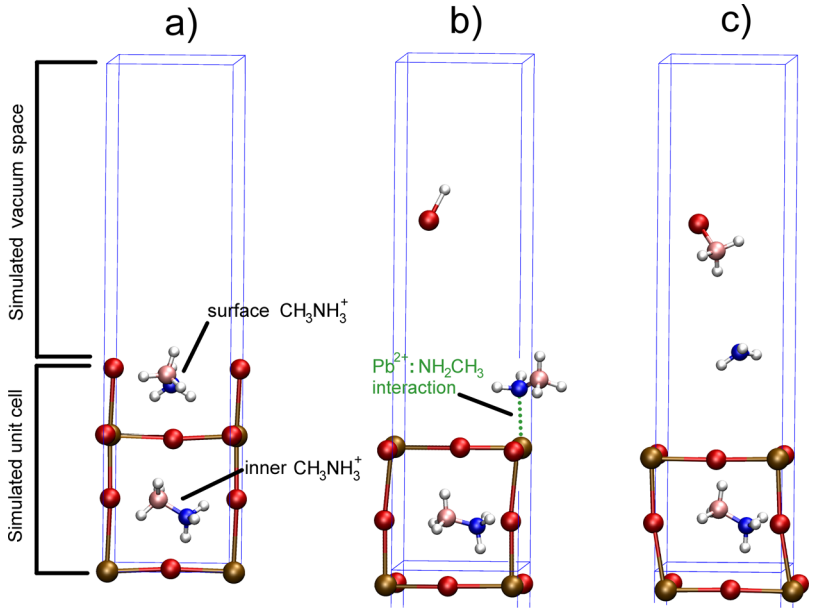

Figure 5. (a) Initial atomic and vacuum space disposition for the $MAPbBr_3$ system. (b) Metadynamics calculations carried out selecting the N−H bond distance as collective variable to simulate deprotonation of methylammonium and production of methylamine and HBr. Main portion of simulated time: methylamine is on the perovskite surface binding its lone electron pair with the electrophilic Pb^{2+} center. (c) Metadynamics calculations carried out selecting the C−N bond distance as collective variable to simulate formation of NH_3 and CH_3Br molecules. In this case, the ammonia molecule separates easily from the perovskite surface.

DOI: 10.1021/acsami.9b02374
ACS Appl. Mater. Interfaces 2019, 11, 12586−12593

simultaneous lower activation energy barrier producing CH_3NH_2 + HI in the left branch and deeper energy valley (*) for CH_3I + NH_3 in the right branch of Figure 4. On the other hand, $MAPbBr_3$ is more stable than $MAPbI_3$ because it releases mostly CH_3NH_2 + HBr at low T. Metadynamics show that it is due to the energy valley in the left branch of Figure 4. This energy valley (#) indicates longer-lived CH_3NH_2 + HX interacting species for X=Br. Simultaneously, $MAPbBr_3$ is less likely to produce CH_3Br + NH_3 because of a shallower energy valley (*) and higher activation energy for the right branch. As it was stated in the previous section, only the CH_3X + NH_3 route can be considered the authentic route of degradation of MA^+ based perovskite.

Metadynamics calculations on solid state surface periodic systems also offered a relevant insight into the course of the metadynamics runs for reaction 4. Upon forming CH_3NH_2 after proton transfer to the X halide, the HX component leaves the perovskite surface. However, CH_3NH_2 remains attached on the surface because the lone electron pair in the N atom donates electronic density to the electrophilic Pb^{2+} center (see Figure 5 and videos in the Supporting Information recording the metadynamics runs).

This tight attachment of CH_3NH_2 staying bonded in the perovskite surface can be rationalized in the framework of the Lewis acid−base theory. CH_3NH_2 is a better nucleophile than NH_3 because the electron donating methyl group attached gives a higher electron density to the electron lone pair of the N atom. Both CH_3NH_2 and NH_3 act as a base, but their pK_a values are 10.6 and 9.3, respectively.[38] The higher nucleophilic character of CH_3NH_2 enables stronger interaction with an electrophilic Pb^{2+} center on the surface. In contrast, the ammonia molecule NH_3 is spelled out from the surface. It has a profound implication in the relative stability of the $MAPbX_3$ perovskite comparing X = Br or I. Br based perovskite is likely to produce CH_3NH_2 + HBr under kinetic conditions as observed experimentally[22] and theoretically in this work. Furthermore, CH_3NH_2 stays preferentially attached on the surface where it is more likely to react back forming again $CH_3NH_3^+$. Both effects explain that $MAPbBr_3$ is a more stable hybrid perovskite than $MAPbI_3$. Noteworthy, a two-parameter empirical stability benchmarking protocol established this stability trend between $MAPbBr_3$ and $MAPbI_3$ recently.[39]

CONCLUSIONS

In summary, we have determined unambiguously by rotational spectroscopy that $MAPbI_3$ may lose the MA^+ cation by two different paths releasing simultaneously (i) CH_3NH_2/HI and (ii) CH_3I/NH_3. Two paths are possible because the quaternary N atom in the MA^+ cation is bonded to two kinds of substituents, protons and methyl moiety. It has been proven experimentally that the neutralization by CH_3NH_2/HI vapors readily back-reacts exclusively to form MAI, not needing a solvent to proceed. Consequently, CH_3NH_2/HI released gases cannot be considered products of degradation of $MAPbI_3$ in a closed system. Contrarily, CH_3I/NH_3 is the authentic detrimental path of degradation because such gaseous release cannot form back selectively to the MA^+/X^- ionic pair. Time-domain atomistic simulations were carried out in the framework of the metadynamics calculations finding that energy barriers connecting MA^+ with release of (i) CH_3NH_2/HX can be considered a kinetic and reversible route while release of (ii) CH_3X/NH_3 is an irreversible reaction being considered as the thermodynamic gas products of MA^+ decomposition. In the same framework of metadynamics calculations, it is found that higher stability of Br based perovskite can be ascribed to (1) the lower Brönsted−Lowry acidity of HBr compared to HI and (2) CH_3NH_2 is a better Lewis base than NH_3. This property makes CH_3NH_2 to stay attached on the electrophilic perovskite surface instead of escaping as seen for the NH_3 molecule. Considering both facts together, namely, long lived HBr molecule and CH_3NH_2 that are prone to stay bonded on the surface, it is more easily understood that MA^+ in $MAPbBr_3$ presents more resistance to be exhausted than MA^+ in $MAPbI_3$.

EXPERIMENTAL SECTION

Neutralization Reaction in Gas Phase Using CH_3NH_2 and HI. A small bottle containing 1 mL (8.04 mmol) of methylamine (CH_3NH_2) solution (33 wt %) in absolute ethanol (Sigma-Aldrich) was placed in a larger closed recipient together with another small bottle containing 1.06 mL (8.04 mmol) of hydroiodic acid (HI) solution (57 wt %) in water (Sigma-Aldrich). After ∼5 min, a polycrystalline white solid ring appeared in the HI containing bottle stuck above the solution interface (see Figure 3a and Figure S2a). After 24 h, the white solid was collected for further characterization using powder XRD.

Menshutkin Reaction (Ammonia Alkylation) in Gas Phase Using CH_3I and NH_3. A similar procedure to above was carried out using two small bottles containing 1 mL (14.72 mmol) of ammonia solution (28 wt %) in water (Sigma-Aldrich) and 0.920 mL of methyliodide (CH_3I) solvent (Sigma-Aldrich, boiling point 42 °C). Both small recipients were enclosed inside a larger recipient. After ∼30 min, a fine white precipitate was observed in the CH_3I solvent. After 24 h, the before bottle containing CH_3I was filled with this fine white solid, and transparent bigger crystals precipitated in the bottom of the NH_3 containing bottle (see Figure 3b and Figure S2b). Both solid products were collected separately for further characterization using powder XRD.

Powder XRD Phase Identification and Quantification. Quantitative phase composition analysis of the samples was carried out using powder X-ray diffraction. Powdered samples were softly ground in a small horizontal vibration mill (CM750 Axel, Japan) for 4 min at 2 Hz using an agate vessel and grinding element. The XRD measurement was performed using a D8 Discover (Bruker AXS GmbH) in a 2θ−ω setup with Cu Kα irradiation, Göbel mirror, and a scintillator detector. Diffraction patterns were collected between 24 and 90° (2θ) in steps of 0.02° with a 5 s accumulation time per step. Quantitative phase composition analysis was done by Rietveld refinement using the BGMN[40] software (www.bgmn.de) with Profex[41] (http://profex. doebelin.org) as the user interface.

$MAPbI_3$ Synthesis. $MAPbI_3$ polycrystalline powder was obtained from $MAPbI_3$ single crystals ground in an agate mortar and pestle. Single crystals were prepared by the inverse temperature crystallization method reported elsewhere.[42] Briefly, 1 M PbI_2 (Sigma-Aldrich, 99%) and MAI (Dyesol Ltd.) solutions were dissolved in γ-butyrolactone at 60 °C under ambient conditions. Subsequently, 2.5 mL of filtered solution using 0.22 μm pore size PTFE filter was transferred to a new 5 mL vial. The new vial was kept in an oil bath at a temperature of 120 °C for 12 h, which induced growth of $MAPbI_3$ crystals.

Rotational Spectroscopy. The analysis of degradation pathways of $MAPbI_3$ was performed in the 6−18 GHz frequency region of a recently built Chirped Pulsed-Fourier Transform Microwave spectrometer (CP-FTMW) at the University of the Basque Country (UPV/EHU). This instrument is based on the original Pate's design. Briefly, a 1 μs chirped pulse was generated in an Arbitrary Waveform Generator, covering 12 GHz. This broadband pulse was frequency-upconverted with a broadband mixer and amplified in a traveling wave tube amplifier (250 W). It was later broadcast inside a high vacuum chamber (evacuable down to 10^{-6} mbar) by using a horn antenna. The excitation induces polarization, resulting in a spontaneous molecular emission signal. This emission was collected with the aid of a second horn antenna and sent to a digital oscilloscope with a 20 GHz bandwidth. For each chirped pulse, a 20 μs time domain signal was recorded in the scope. In the current setup, 30 chirped pulses were used in each molecular pulse. The perovskite sample was placed in a customized

DOI: 10.1021/acsami.9b02374
ACS Appl. Mater. Interfaces 2019, 11, 12586−12593

heating nozzle and heated to maximize the release of gases thanks to a resistance heating wire. The nozzle was attached to a pulsed solenoid valve, and a carrier gas (helium) was flown through it. The $MAPbI_3$ polycrystalline powder was progressively heated until 230 °C (in steps of 20 °C) to generate faster an enough quantity of decomposition gases. In this way, the gas detection was assured avoiding Menshutkin reaction and acid−base neutralization to react back to solid products impeding gas detection. After measurement, the initially black perovskite sample was found fully converted to the yellowish PbI_2 after 70 h of measurement inside the chamber. In our current setup, it is not possible to detect the other plausible gaseous products (HI and NH_3) because they do not possess rotational transitions in the working frequency range of our spectrometer (6−18 GHz). In fact, the lowest transitions for these two species are located at 385 GHz for HI[43] and 572 GHz for NH_3[44] well beyond the upper-frequency limit of our apparatus.

Metadynamics Calculations in Periodic System. Car−Parrinello molecular dynamics (CPMD) simulations[45] in the canonical ensemble were performed for a $MAPbX_3$ surface (100) plane interfacing 20 Å vacuum space using the pseudopotential plane-wave density functional theory module implemented in NWChem 6.6.[46] The exchange-correlation functional used was Perdew−Burke−Ernzerhof revised for solids (PBEsol) including Grimme dispersion corrections (PBEsol-Grimme4).[47] The periodic simulated system of choice consists of the cubic phase of $MAPbX_3$. Each structure was initially equilibrated for 5 ps at 340 K (Nose−Hoover thermostat) prior to metadynamics calculations. Starting with equilibrated CPMD geometries, the metadynamics simulations were carried out using as a collective variable the breaking bond of choice according to reaction 4 or 5. A gaussian was added every 100 time steps. The total collection time for each simulation was 1100 ps. Drawings and movies of molecules were obtained using a combination of VMD,[48] the PyMOL Molecular Graphics System (Version 1.7.4, Schrödinger, LLC), and Gabedit 2.4.8.[49] Four short video films showing metadynamics calculations on $MAPbI_3$ and $MAPbBr_3$ surfaces along the reaction coordinates (reactions 4 and 5) have been deposited in the Supporting Information.

■ ASSOCIATED CONTENT

Supporting Information

The Supporting Information is available free of charge on the ACS Publications website at DOI: 10.1021/acsami.9b02374.

Gas phase reaction to solid ammonium salt experiment pictures using CH_3NH_2 + HI and CH_3I + NH_3 as gas precursors. Powder XRD diffractogram survey of the solid products obtained. DFT calculations on simplified model reaction. Global optimization of isolated ionic pair system $MA^+\cdots X^-$ at DFT level and metadynamics calculations in isolated system $MA^+\cdots X^-$. Temperature dependent mass spectrometry measurement of gas species released under low temperature pulsed heating test (PDF)

Four short video films showing metadynamics calculations on $MAPbI_3$ and $MAPbBr_3$ surfaces along the reaction coordinate (ZIP)

■ AUTHOR INFORMATION

Corresponding Authors

*E-mail: ejjuarezperez@gmail.com (E.J.J.-P.).
*E-mail: Yabing.Qi@OIST.jp (Y.Q.).

ORCID

Emilio J. Juarez-Perez: 0000-0001-6040-1920
Emilio J. Cocinero: 0000-0001-7632-3728
Yabing Qi: 0000-0002-4876-8049

Notes

The authors declare no competing financial interest.

■ ACKNOWLEDGMENTS

This work was supported by funding from the Energy Materials and Surface Sciences Unit of the Okinawa Institute of Science and Technology Graduate University, the OIST Proof of Concept (POC) Program, the OIST R&D Cluster Research Program, JSPS KAKENHI Grant number JP18K05266 (YBQ), and JSPS KAKENHI Young B Grant Number 17 K14551 (EJJ-P). We thank MINECO project (CTQ2017-89150-R) and the UPV/EHU (PPG17/10) for financial support. I.U. acknowledges the Spanish Government for an FPU contract. Computational and laser resources of the UPV/EHU were used in this work (SGIker and I2Basque).

■ REFERENCES

(1) Yang, Y.; You, J. Make perovskite solar cells stable. *Nature* **2017**, *544*, 155−156.
(2) Hashmi, S. G.; Tiihonen, A.; Martineau, D.; Ozkan, M.; Vivo, P.; Kaunisto, K.; Ulla, V.; Zakeeruddin, S. M.; Grätzel, M. Long term stability of air processed inkjet infiltrated carbon-based printed perovskite solar cells under intense ultra-violet light soaking. *J. Mater. Chem. A* **2017**, *5*, 4797−4802.
(3) Grancini, G.; Roldán-Carmona, C.; Zimmermann, I.; Mosconi, E.; Lee, X.; Martineau, D.; Narbey, S.; Oswald, F.; De Angelis, F.; Graetzel, M.; Nazeeruddin, M. K. One-Year stable perovskite solar cells by 2D/3D interface engineering. *Nat. Commun.* **2017**, *8*, 15684.
(4) Ono, L. K.; Juarez-Perez, E. J.; Qi, Y. Progress on perovskite materials and solar cells with mixed cations and halide anions. *ACS Appl. Mater. Interfaces* **2017**, *9*, 30197−30246.
(5) Kojima, A.; Teshima, K.; Shirai, Y.; Miyasaka, T. Organometal Halide Perovskites as Visible-Light Sensitizers for Photovoltaic Cells. *J. Am. Chem. Soc.* **2009**, *131*, 6050−6051.
(6) NREL *Best Research-Cell Efficiencies*. https://www.nrel.gov/pv/assets/images/efficiency-chart-20180716.jpg (accessed on July 20th, 2018).
(7) Conings, B.; Drijkoningen, J.; Gauquelin, N.; Babayigit, A.; D'Haen, J.; D'Olieslaeger, L.; Ethirajan, A.; Verbeeck, J.; Manca, J.; Mosconi, E.; De Angelis, F.; Boyen, H.-G. Intrinsic Thermal Instability of Methylammonium Lead Trihalide Perovskite. *Adv. Energy Mater.* **2015**, *5*, 1500477.
(8) Ramos, F. J.; Maindron, T.; Bèchu, S.; Rebai, A.; Frègnaux, M.; Bouttemy, M.; Rousset, J.; Schulz, P.; Schneider, N. Versatile perovskite solar cell encapsulation by low-temperature ALD-Al_2O_3 with long-term stability improvement. *Sustainable Energy Fuels* **2018**, *2*, 2468−2479.
(9) Huang, H.; Chen, B.; Wang, Z.; Hung, T. F.; Susha, A. S.; Zhong, H.; Rogach, A. L. Water resistant $CsPbX_3$ nanocrystals coated with polyhedral oligomeric silsesquioxane and their use as solid state luminophores in all-perovskite white light-emitting devices. *Chem. Sci.* **2016**, *7*, 5699−5703.
(10) Frost, J. M.; Butler, K. T.; Brivio, F.; Hendon, C. H.; van Schilfgaarde, M.; Walsh, A. Atomistic Origins of High-Performance in Hybrid Halide Perovskite Solar Cells. *Nano Lett.* **2014**, *14*, 2584−2590.
(11) Deretzis, I.; Alberti, A.; Pellegrino, G.; Smecca, E.; Giannazzo, F.; Sakai, N.; Miyasaka, T.; La Magna, A. Atomistic origins of $CH_3NH_3PbI_3$ degradation to PbI_2 in vacuum. *Appl. Phys. Lett.* **2015**, *106*, 131904.
(12) Dualeh, A.; Gao, P.; Seok, S. I.; Nazeeruddin, M. K.; Grätzel, M. Thermal Behavior of Methylammonium Lead-trihalide Perovskite Photovoltaic Light Harvesters. *Chem. Mater.* **2014**, *26*, 6160−6164.
(13) Nenon, D. P.; Christians, J. A.; Wheeler, L. M.; Blackburn, J. L.; Sanehira, E. M.; Dou, B.; Olsen, M. L.; Zhu, K.; Berry, J. J.; Luther, J. M. Structural and chemical evolution of methylammonium lead halide perovskites during thermal processing from solution. *Energy Environ. Sci.* **2016**, *9*, 2072−2082.
(14) Leguy, A. M. A.; Hu, Y.; Campoy-Quiles, M.; Alonso, M. I.; Weber, O. J.; Azarhoosh, P.; van Schilfgaarde, M.; Weller, M. T.; Bein, T.; Nelson, J.; Docampo, P.; Barnes, P. R. F. Reversible Hydration of

DOI: 10.1021/acsami.9b02374
ACS Appl. Mater. Interfaces 2019, 11, 12586−12593

$CH_3NH_3PbI_3$ in Films, Single Crystals, and Solar Cells. *Chem. Mater.* **2015**, *27*, 3397−3407.
(15) Philippe, B.; Park, B.-W.; Lindblad, R.; Oscarsson, J.; Ahmadi, S.; Johansson, E. M. J.; Rensmo, H. Chemical and Electronic Structure Characterization of Lead Halide Perovskites and Stability Behavior under Different Exposures - A Photoelectron Spectroscopy Investigation. *Chem. Mater.* **2015**, *27*, 1720−1731.
(16) Khadka, D. B.; Shirai, Y.; Yanagida, M.; Miyano, K. Degradation of encapsulated perovskite solar cells driven by deep trap states and interfacial deterioration. *J. Mater. Chem. C* **2018**, *6*, 162−170.
(17) Juarez-Perez, E. J.; Hawash, Z.; Raga, S. R.; Ono, L. K.; Qi, Y. Thermal degradation of $CH_3NH_3PbI_3$ perovskite into NH_3 and CH_3I gases observed by coupled thermogravimetry - mass spectrometry analysis. *Energy Environ. Sci.* **2016**, *9*, 3406−3410.
(18) Williams, A. E.; Holliman, P. J.; Carnie, M. J.; Davies, M. L.; Worsley, D. A.; Watson, T. M. Perovskite processing for photovoltaics: a spectro-thermal evaluation. *J. Mater. Chem. A* **2014**, *2*, 19338−19346.
(19) Xu, W.; McLeod, J. A.; Yang, Y.; Wang, Y.; Wu, Z.; Bai, S.; Yuan, Z.; Song, T.; Wang, Y.; Si, J.; Wang, R.; Gao, X.; Zhang, X.; Liu, L.; Sun, B. Iodomethane-Mediated Organometal Halide Perovskite with Record Photoluminescence Lifetime. *ACS Appl. Mater. Interfaces* **2016**, *8*, 23181−23189.
(20) Latini, A.; Gigli, G.; Ciccioli, A. A study on the nature of the thermal decomposition of methylammonium lead iodide perovskite, $CH_3NH_3PbI_3$: an attempt to rationalise contradictory experimental results. *Sustainable Energy Fuels* **2017**, 1351−1357.
(21) Xu, W.; Liu, L.; Yang, L.; Shen, P.; Sun, B.; McLeod, J. A. Dissociation of Methylammonium Cations in Hybrid Organic-Inorganic Perovskite Solar Cells. *Nano Lett.* **2016**, *16*, 4720−4725.
(22) Juarez-Perez, E. J.; Ono, L. K.; Maeda, M.; Jiang, Y.; Hawash, Z.; Qi, Y. Photodecomposition and thermal decomposition in methylammonium halide lead perovskites and inferred design principles to increase photovoltaic device stability. *J. Mater. Chem. A* **2018**, *6*, 9604−9612.
(23) Gordy, W.; Cook, R. L. *Microwave Molecular Spectra*. Wiley: New York, 1984.
(24) Cocinero, E. J.; Lesarri, A.; Écija, P.; Basterretxea, F. J.; Grabow, J.-U.; Fernández, J. A.; Castaño, F. Ribose Found in the Gas Phase. *Angew. Chem. Int. Ed.* **2012**, *51*, 3119−3124.
(25) Uriarte, I.; Melandri, S.; Maris, A.; Calabrese, C.; Cocinero, E. J. Shapes, Dynamics, and Stability of β-Ionone and Its Two Mutants Evidenced by High-Resolution Spectroscopy in the Gas Phase. *J. Phys. Chem. Lett.* **2018**, *9*, 1497−1502.
(26) Guo, X.; McCleese, C.; Kolodziej, C.; Samia, A. C. S.; Zhao, Y.; Burda, C. Identification and characterization of the intermediate phase in hybrid organic-inorganic $MAPbI_3$ perovskite. *Dalton Trans.* **2016**, *45*, 3806−3813.
(27) Ilyushin, V.; Lovas, F. J. Microwave spectra of molecules of astrophysical interest. XXV. Methylamine. *J. Phys. Chem. Ref. Data* **2007**, *36*, 1141−1276.
(28) Young, S. H.; Kukolich, S. G. Microwave measurements and calculations of quadrupole coupling effects in CH_3I and CD_3I. *J. Mol. Spectrosc.* **1985**, *114*, 483−493.
(29) Lee, M. M.; Teuscher, J.; Miyasaka, T.; Murakami, T. N.; Snaith, H. J. Efficient Hybrid solar cells based on meso-superstructured Organometal Halide Perovskites. *Science* **2012**, *338*, 643−647.
(30) Chen, Q.; Zhou, H.; Hong, Z.; Luo, S.; Duan, H.-S.; Wang, H.-H.; Liu, Y.; Li, G.; Yang, Y. Planar heterojunction perovskite solar cells via vapor-assisted solution process. *J. Am. Chem. Soc.* **2014**, *136*, 622−625.
(31) Raga, S. R.; Ono, L. K.; Qi, Y. Rapid perovskite formation by CH_3NH_2 gas-induced intercalation and reaction of PbI_2. *J. Mater. Chem. A* **2016**, *4*, 2494−2500.
(32) Pang, S.; Zhou, Y.; Wang, Z.; Yang, M.; Krause, A. R.; Zhou, Z.; Zhu, K.; Padture, N. P.; Cui, G. Transformative Evolution of Organolead Triiodide Perovskite Thin Films from Strong Room-Temperature Solid-Gas Interaction between $HPbI_3$-CH_3NH_2 Precursor Pair. *J. Am. Chem. Soc.* **2016**, *138*, 750−753.
(33) Long, M.; Zhang, T.; Chai, Y.; Ng, C.-F.; Mak, T. C. W.; Xu, J.; Yan, K. Nonstoichiometric acid-base reaction as reliable synthetic route to highly stable $CH_3NH_3PbI_3$ perovskite film. *Nat. Commun.* **2016**, *7*, 13503.
(34) Ke, J. C.-R.; Walton, A. S.; Lewis, D. J.; Tedstone, A.; O'Brien, P.; Thomas, A. G.; Flavell, W. R. In situ investigation of degradation at organometal halide perovskite surfaces by X-ray photoelectron spectroscopy at realistic water vapour pressure. *Chem. Commun.* **2017**, *53*, 5231−5234.
(35) Ensing, B.; De Vivo, M.; Liu, Z.; Moore, P.; Klein, M. L. Metadynamics as a Tool for Exploring Free Energy Landscapes of Chemical Reactions. *Acc. Chem. Res.* **2006**, *39*, 73−81.
(36) Laio, A.; Gervasio, F. L. Metadynamics: a method to simulate rare events and reconstruct the free energy in biophysics, chemistry and material science. *Rep. Prog. Phys.* **2008**, *71*, 126601.
(37) Michel, C.; Laio, A.; Milet, A. Tracing the Entropy along a Reactive Pathway: The Energy As a Generalized Reaction Coordinate. *J. Chem. Theory Comput.* **2009**, *5*, 2193−2196.
(38) Dean, J. A. *Lange's Handbook of Chemistry*, 15th ed.; McGraw Hill Book Co.: New York, NY, 1999.
(39) García-Fernández, A.; Juarez-Perez, E. J.; Castro-García, S.; Sánchez-Andújar, M.; Ono, L. K.; Jiang, Y.; Qi, Y. Benchmarking chemical stability of arbitrarily mixed 3D hybrid halide perovskites for solar cell applications. *Small Methods* **2018**, 1800242.
(40) Bergmann, J.; Friedel, P.; Kleeberg, R. BGMN - A new fundamental parameters based Rietveld program for laboratory X-ray sources, its use in quantitative analysis and structure investigations. *CPD Newsl.* **1998**, *20*, 5−8.
(41) Doebelin, N.; Kleeberg, R. Profex: a graphical user interface for the Rietveld refinement program BGMN. *J. Appl. Crystallogr.* **2015**, *48*, 1573−1580.
(42) Saidaminov, M. I.; Abdelhady, A. L.; Murali, B.; Alarousu, E.; Burlakov, V. M.; Peng, W.; Dursun, I.; Wang, L.; He, Y.; Maculan, G.; Goriely, A.; Wu, T.; Mohammed, O. F.; Bakr, O. M. High-quality bulk hybrid perovskite single crystals within minutes by inverse temperature crystallization. *Nat. Commun.* **2015**, *6*, 7586.
(43) De Lucia, F. C.; Helminger, P.; Gordy, W. Submillimeter-wave spectra and equilibrium structures of the hydrogen halides. *Phys. Rev. A* **1971**, *3*, 1849.
(44) Helminger, P.; De Lucia, F. C.; Gordy, W. Rotational spectra of NH_3 and ND_3 in the 0.5-mm wavelength region. *J. Mol. Spectrosc.* **1971**, *39*, 94−97.
(45) Car, R.; Parrinello, M. Unified approach for molecular dynamics and density-functional theory. *Phys. Rev. Lett.* **1985**, *55*, 2471.
(46) Valiev, M.; Bylaska, E. J.; Govind, N.; Kowalski, K.; Straatsma, T. P.; Van Dam, H. J. J.; Wang, D.; Nieplocha, J.; Apra, E.; Windus, T. L.; de Jong, W. A. NWChem: A comprehensive and scalable open-source solution for large scale molecular simulations. *Comput. Phys. Commun.* **2010**, *181*, 1477−1489.
(47) Grimme, S.; Ehrlich, S.; Goerigk, L. Effect of the damping function in dispersion corrected density functional theory. *J. Comput. Chem.* **2011**, *32*, 1456−1465.
(48) Humphrey, W.; Dalke, A.; Schulten, K. VMD: Visual Molecular Dynamics. *J. Mol. Graphics* **1996**, *14*, 33−38.
(49) Allouche, A.-R. Gabedit - A graphical user interface for computational chemistry softwares. *J. Comput. Chem.* **2011**, *32*, 174−182.

DOI: 10.1021/acsami.9b02374
ACS Appl. Mater. Interfaces 2019, 11, 12586−12593